Optics Letters

Efficient all-solid-state passively *Q*-switched SWIR Tm:YAP/KGW Raman laser

Eytan Perez,[1] Uzziel Sheintop,[1] Rotem Nahear,[1] Gilad Marcus,[2] and Salman Noach[1,*]

[1]*Department of Applied Physics, Electro-optics Engineering Faculty, Jerusalem College of Technology, Jerusalem, Israel*
[2]*Department of Applied Physics, The Hebrew University of Jerusalem, Jerusalem, Israel*
Corresponding author: salman@jct.ac.il

We present an all-passive efficient KGW Raman laser with an external-cavity configuration in the 2 µm spectral regime. The Raman laser was pumped by a passively *Q*-switched Tm:YAP laser emitting at 1935 nm. Due to the bi-axial properties of the KGW crystal, the laser exhibits stimulated Raman emission at two separate spectral lines: 2272 nm and 2343 nm. The output energies achieved at these two lines are 340 µJ/pulse and 450 µJ/pulse, accordingly. The seed to Raman laser conversion efficiencies achieved of 19.2% and 23.5%, respectively, are comparable to actively *Q*-switched laser arrangements. To the best of our knowledge, this is the first time an efficient Raman laser in the 2 µm regime is demonstrated in a completely passive configuration.   © 2020 Optical Society of America

https://doi.org/10.1364/OL.401833

Over the last two decades, high brightness sources in the 2-3 µm regime have become essential in many fields of applications, including microsurgery, polymers and metals processing, gas monitoring, LIDAR as well as defense applications [1–4]. Although the rare-earth ions such as thulium, holmium, and chromium, allow for such laser sources, they do not cover this entire spectral range. The stimulated Raman scattering (SRS) effect is a well-known and efficient non-linear technique commonly used to convert visible or short-wave infrared (SWIR) wavelengths to longer wavelengths by single or multiple Stokes transitions. Solid-state Raman lasers are one of the most efficient methods enabling the extension of the spectral span of high brightness sources [5–7]. This approach was also recognized in the 2 µm spectral regime, using $BaWO_4$ and YVO_4 crystals as Raman gain medium [8,9]. Some of these efforts include compact laser sources, which are being developed to address the increasing demand for high-power SWIR lasers covering this spectral regime [2,10].

Raman lasers have several advantages and features–from pulse length shortening to the improvement of spatial beam quality by Raman beam cleanup. Since the SRS gain coefficient is inversely proportional to the wavelength, Raman lasers are implemented mostly in the visible and near-infrared (NIR) regimes, but not often in the SWIR spectral regime [7]. Based on the increase in peak power demonstrated over the past years for Tm-doped

and Ho-doped solid-state lasers in the 2 µm regime [3,11], SRS could achieve relatively high conversion efficiencies. This approach could indeed be a viable method to obtain SWIR wavelengths otherwise difficult to achieve.

Among the well-known and used SRS-capable crystals ($LiLO_3$, $CaWO_4$, $Ba(NO_3)_2$, YVO_4 and $BaWO_4$), one of the most popular Raman crystals is the potassium gadolinium tungstate ($KGd(WO_4)_2$ or KGW) owing to its attractive thermal properties, high damage threshold, as well as a highly integrated scattering cross-section [5]. Inherently, the KGW is a bi-axial crystal, which for a b-axis cut has an SRS interaction with two vibrational modes at $768\,cm^{-1}$ and $901\,cm^{-1}$, allowing separate Raman lasing in two independent first order Stokes lines by controlling the polarization direction of the seed laser [12].

According to a previous study in our group, the Raman gain coefficient of the KGW around 1.9 µm is estimated at 1.0 cm/GW and 0.9 cm/GW for the $768\,cm^{-1}$ and $901\,cm^{-1}$ vibrational modes accordingly [10]. In comparison to the well-known $BaWO_4$ Raman crystal, which, according to [13], has an estimated 1.1 cm/GW gain coefficient at 1.94 µm, the KGW crystal has a higher damage threshold, thus compensating the slightly lower gain coefficient by being able to sustain higher seed density.

The majority of the studies done in this field are based on active *Q*-switching (AQS) approaches. Although these techniques allow complete control over the seed repetition rate, they are bulky, energy-consuming, and much more expensive to produce than a compact, passive *Q*-switching (PQS) architecture. The use of Cr:ZnS and Cr:ZnSe crystal as saturable absorber (SA) for PQS is a common technique used in the SWIR regime. It allows one to achieve relatively high energies and short pulse durations [11,14].

Several studies have been carried out in the Raman-based SWIR spectral regime. In 2002, a self-frequency modulated Raman laser achieved a couple of µJ at 2365 nm due to low conversion efficiency [15]. Since then, the efficiency of SWIR Raman lasers has continually improved. Recently, our group reported an external cavity architecture Tm:YLF/KGW based on an AQS modulation. This laser exhibited a conversion efficiency of 20% with a maximal energy of 0.4 mJ, and an average
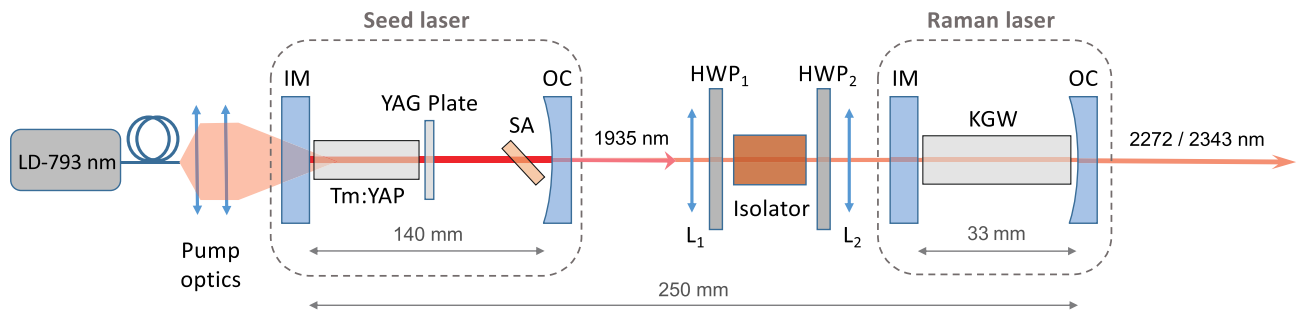
Fig. 1. Experimental setup schematic of the Tm:YAP seed coupled to the external KGW Raman laser: LD, laser diode; IM, input mirror; OC, output coupler; SA, saturable absorber; (HWP$_1$ & HWP$_2$), half waveplates; (L$_1$ & L$_2$), collimating and focusing lenses.

power of 400 mW [10]. In 2019, an AQS Tm:YLF/diamond-based design presented efficiency as high as 38%, but still with limited average power at around 8 mW at a slow repetition rate of 5 Hz [16].

In this Letter, we report the results of the investigation conducted on an end-pumped, passively *Q*-switched, external cavity, KGW Raman laser operating in the SWIR regime at 2272 nm and 2343 nm, exhibiting a highly efficient seed-to-Raman conversion efficiency as high as 19.2% and 23.5% accordingly. To the best of our knowledge, this is the first efficient all-solid-state PQS KGW Raman-based laser operating in the 2 μm spectral regime.

The experimental setup of the Raman laser and its seed is shown in Fig. 1. The seed laser is based on a linear end-pumped design developed in our group [14], with a $3 \times 3 \times 10$ mm^3 b-cut Tm:YAP (3.5% at.) crystal as the gain medium. Although the former design achieved relatively high energies, some modifications were needed to achieve higher peak power. First, the resonator length was shortened, and second, a $6 \times 7 \times 2$ mm^3 uncoated 80% transparent Cr:ZnS SA crystal was held at the Brewster angle. The latter allowed for a much higher damage threshold inside the seed cavity, enabling stronger and shorter pulses. The gain medium was pumped by a 793 nm fiber-coupled laser diode with a 105 μm core diameter and an NA of 0.22. Both the diode and the Tm:YAP crystal were water-cooled to 19°C. The input mirror (IM) of the Tm:YAP cavity is a flat mirror, coated for high transmission at 793 nm and highly reflective (HR) around 1900 nm. A partially reflecting (PR) coated at 55% reflectance around 1900 nm output-coupler (OC) with a 200 mm radius of curvature (ROC) was placed 140 mm from the IM. The 793 nm laser-diode pump was collimated and focused inside the Tm:YAP crystal using two anti-reflecting (AR) coated lenses to a spot diameter of 240 μm. As depicted in Fig. 2, the PQS Tm:YAP laser exhibited up to 2 W of average output power for an absorbed pump power of 10.7 W, at a repetition rate of 1 kHz. An energy pulse of 2 mJ for a pulse duration of 14.7 ns (FWHM), corresponding to a maximal peak power of 142.8 kW was measured.

Besides the need for a high peak-power pump on the KGW crystal, other laser characteristics are required to achieve a Raman gain high enough to allow SRS generation: good beam quality, linear polarization matching with the KGW crystal's axis, as well as narrow spectral bandwidth [17,18]. It should be mentioned that without narrowing the natural Tm:YAP spectral bandwidth no SRS could have been observed. The seed spectral peak location was at 1935 nm, as depicted in Fig. 3.
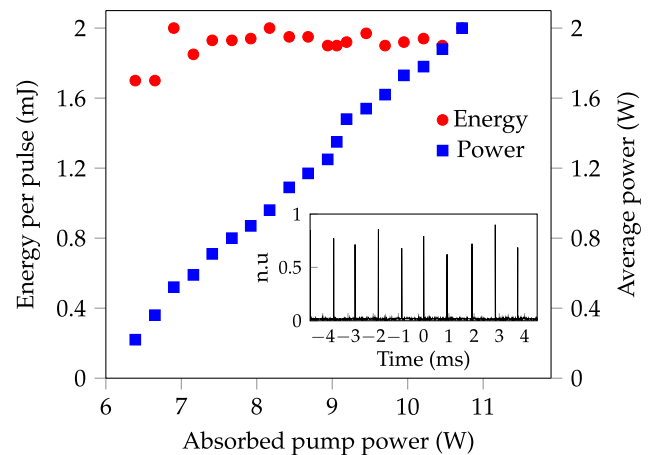

Fig. 2. Seed Tm:YAP laser performances, with the corresponding pulse train as depicted from inset.

The seed spectral bandwidth was narrowed from ~1.4 nm down to ~0.2 nm. This was achieved due to the 100 μm thick uncoated yttrium aluminum garnet (YAG) etalon plate, which was placed adjacent to the Tm:YAP crystal. All the seed laser characteristics mentioned above were measured after the induced losses by the optical delivery components prior to the Raman cavity. These components were two anti-reflective (AR)-coated lenses (L$_1$ & L$_2$), an optical isolator, two half-wave plates (HWP$_1$ & HWP$_2$), as well as two additional silver-coated folding mirrors.

The Tm:YAP laser beam was imaged using L$_1$ & L$_2$, to a ~180 μm spot diameter inside the KGW Raman crystal. HWP$_2$ was added after the isolator, to control the seed's polarization orientation prior to the KGW cavity. This allowed switching between the two different Raman vibration shifts of the KGW crystal, enabling us to alternate selectively between 2272 nm and 2343 nm.

A plano mirror, AR coated at the seed wavelength and HR coated between 2200–2700 nm, was used as an IM for the Raman laser cavity, and a mirror with a 200 mm ROC was used as an OC. This OC was PR coated to 90% reflectance between 2200–2700 nm, and was also HR coated at the seed wavelength, forcing a double-pass of the seed laser beam inside the Raman cavity. A $7 \times 7 \times 30$ mm^3 KGW crystal was used as an active Raman medium, and both facets were AR coated at the seed wavelength. The crystal was oriented for propagation along the

b-axis, having 901 cm^{-1} and 768 cm^{-1} shifts for the E (electric field) direction, being perpendicular to the c-axis and a-axis, respectively [12]. As depicted in Fig. 1, the total Raman laser cavity length is 33 mm. The Raman laser beam diameter inside the KGW crystal was calculated by the ABCD matrix method to be 395 µm and 405 µm at 2272 nm and 2343 nm, respectively. This mode matching (between the seed and the Raman laser) was found to be highly efficient, as previously mentioned in Ref. [10].

The pulse energy was measured using an energy meter (Ophir, PE50-C). Pulse temporal characterization was performed using an extended InGaAs fast photo-detector (ALPHALAS, UPD-5N-IR2-P) and an oscilloscope (Agilent, DSO-X 2012A). The laser spectrum was acquired by a spectrometer (APE, waveScan). Spatial profiling of the laser beam was performed using a pyroelectric camera (Spiricon, Pyrocam III-HR).

The Raman laser output spectra shown in Fig. 3, which presents the two separate emission lines at 2272 nm and 2343 nm, matches the two expected Stokes shifts from the seed 1935 nm wavelength. The two lines are observed separately by rotating the polarization between the two Raman shift axes (orthogonal to each other) of the KGW crystal, in agreement with [7]. Because of this system's PQS nature, it was not possible to synchronize the camera to the laser sampling frequency well enough. In addition to that, any attempts for measuring the M^2 using the pinhole method were not successful because of the Raman laser pulse-to-pulse energy instabilities. However, when measuring the seed in the CW configuration (by removing the
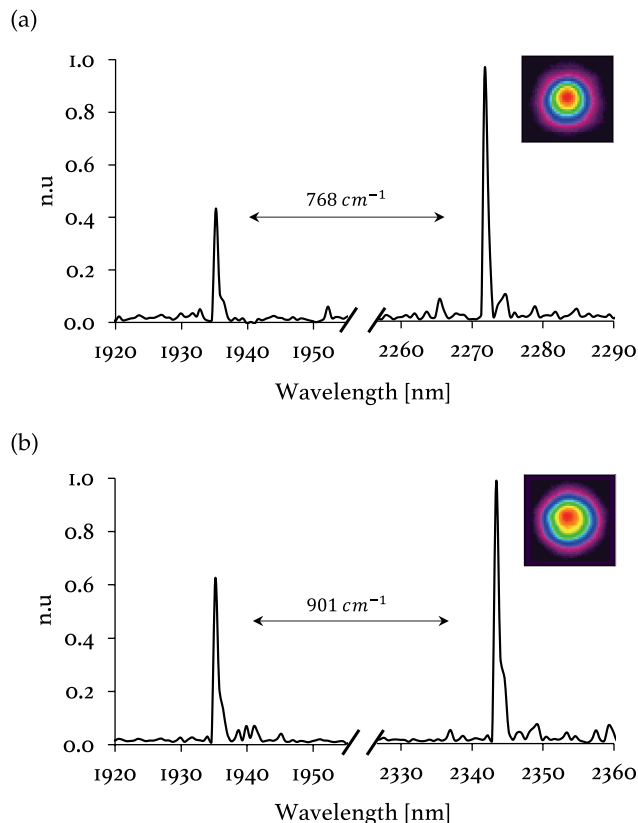
(a)

(b)

Fig. 3. KGW Raman spectral shifts (768 cm^{-1} and 901 cm^{-1}) from 1935 nm to 2272 nm (a) and 2343 nm (b) with their corresponding beam profiles respectively.
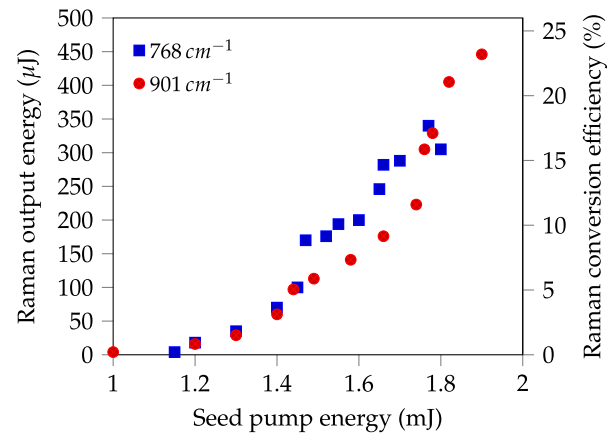

Fig. 4. Raman KGW energy pulse and optical-to-optical conversion efficiency versus seed energy input at a 1 kHz repetition rate, for the two orthogonal Raman shifts.

SA), the obtained M^2 was 1.1. According to [7,19], it is unlikely that the Raman Stokes M^2 will be worse than the M^2 of the seed. Nevertheless, we were able to sample the beam profiles for each of the Stokes shift, as depicted in Fig. 3. The spectral bandwidth measured here is 1 nm at FWHM. In reality, the spectral bandwidths of the seed and the Raman laser beams are likely narrower, following [10,14]. This was mainly due to the 0.5 nm spectrometer's resolution at this spectral regime.

The output energy, average power, and conversion efficiencies for the two orthogonal first order Raman shifts can be seen in Fig. 4. During the Raman characterization, the seed laser was pumped at constant power. This approach was chosen to hold a constant repetition rate and pulse duration at 1 kHz and 14.7 ns accordingly. The seed laser was then optically attenuated by rotating HWP$_1$ relative to the isolator's entrance polarizer cube. This technique allowed us to modify the seed pulse energy, allowing the characterization of the KGW resonator for both Raman shifts. The optimal results obtained for the Raman shifts are listed in Table 1.

As mentioned above, Fig. 4 shows the conversion efficiency of the orthogonal first Stokes to the seed laser. It can be seen that the efficiencies for both shifts stay very similar up to a seed pulse energy of 1.5 mJ. As demonstrated by [20], and in agreement with the experimental results of [10], the 768 cm^{-1} shift corresponding to the shorter spectral shift has higher conversion efficiency up to 1.8 mJ of seed pulse energy. From here, the longer shift (901 cm^{-1}) starts to overtake the shorter shift (768 cm^{-1}) with respect to the energy per pulse and the conversion efficiency. We estimate that due to the higher gain coefficient for the 768 cm^{-1} shift, another nonlinear process arises, lowering the overall SRS efficiency while introducing high peak-power pulses for this vibrational mode.

Figure 5 shows the reduction in pulse width from the undepleted seed pulse (14.7 ns) to the Stokes pulse (13 ns) at both Raman shifts. These curves represent the averaged temporal samplings over one minute, at a repetition rate of 1 kHz. It should be mentioned that these temporal characteristics were not measured at maximum performance as appearing in Fig. 4. Moreover, the depleted seed beam measured after double passing in the KGW cavity has been temporally shifted in post-processing to match the undepleted pulse rising edge. After reaching the SRS threshold (at around 50 kW peak power), the

Table 1.   KGW Raman Laser Maximal Performances for the Two Raman Shifts Stokes

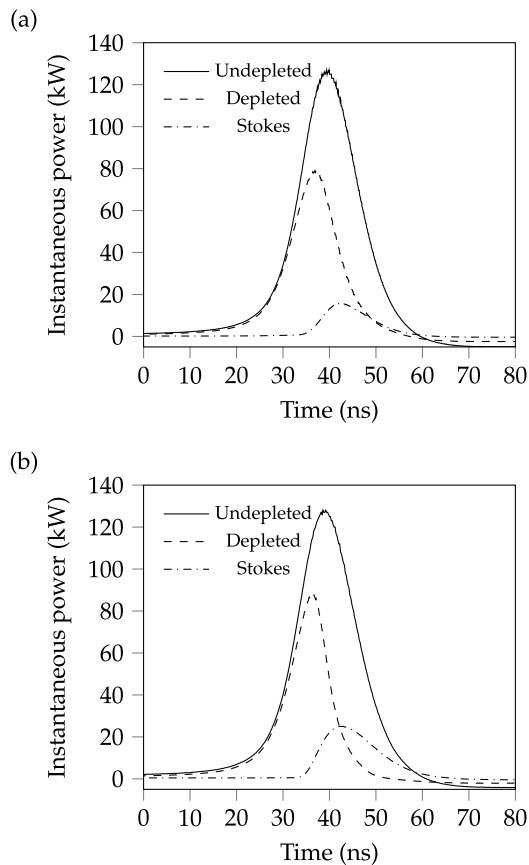| Shift	Wavelength	Energy	Pulse Duration	Peak-power	Efficiency$_{energy}$	Power	Slope Efficiency
768 cm^{-1}	2272 nm	340 μJ/pulse	13 ns	26.1 kW	19.2%	340 mW	54.6%
901 cm^{-1}	2342 nm	446 μJ/pulse	13 ns	34.3 kW	23.5%	446 mW	62.2%

(a)

(b)

Fig. 5. Measurement of the temporal characteristics for the undepleted, depleted, and Stokes pulses for the 768 cm^{-1} and 901 cm^{-1} Raman shifts, (a) and (b) accordingly.

Raman laser energy increases, while the pump laser energy is shown to decrease towards the depleted seed case.

In conclusion, we present in this Letter the highest performance of a PQS-based design Raman laser. Notably, this all-solid PQS Raman laser is superior to AQS Raman architectures in terms of energy pulse, average power, pulse duration, and conversion efficiency. The KGW Raman active medium was pumped using a 1935 nm PQS Tm:YAP laser. The two orthogonal Raman shifts (768 cm^{-1} and 901 cm^{-1}) have successfully shifted the seed laser by emitting at 2272 nm and 2343 nm separately, exhibiting 340 μJ and 446 μJ pulse energies accordingly, both having a pulse duration of 13 ns. This Raman laser achieved a seed-to-Raman conversion efficiency as high as 19.2% and 23.5% for the two Raman vibrational modes accordingly.

To the best of our knowledge, this is the first implementation of an efficient all-solid-state, passively *Q*-switched Raman laser. We have shown that the KGW is suitable for an efficient SRS conversion to the SWIR spectral regime. The high pulse energies achieved prove that a compact and robust PQS architecture is particularly suitable for efficient lasing in the 2200–2300 nm spectral range, which is otherwise difficult to achieve. These results from an all-solid, compact architecture open new possibilities for many applications in the medical, remote sensing, LIDAR, as well as defense fields.

REFERENCES

1. I. Sorokina and K. Vodopyanov, *Solid-state Mid-infrared Laser Sources* (Springer, 2003).
2. A. Godard, C. R. Phys. **8**, 1100 (2007).
3. K. Scholle, S. Lamrini, P. Koopmann, and P. Fuhrberg, *Frontiers in Guided Wave Optics and Optoelectronics* (InTech, 2010).
4. L. Guillemot, P. Loiko, A. Braud, J.-L. Doualan, A. Hideur, M. Koselja, R. Moncorge, and P. Camy, Opt. Lett. **44**, 5077 (2019).
5. J. A. Piper and H. M. Pask, IEEE J. Sel. Top. Quantum Electron. **13**, 692 (2007).
6. P. Cerný, H. Jelinkov, P. G. Zverevb, and T. T. Basievb, Prog. Quantum Electron. **28**, 113 (2004).
7. H. Pask, Prog. Quantum Electron. **27**, 3 (2003).
8. O. Kuzucu, Opt. Lett. **40**, 5078 (2015).
9. P. Cheng, J. Zhao, F. Xu, X. Zhou, and G. Wang, Appl. Phys. B **124**, 5 (2017).
10. U. Sheintop, D. Sebbag, P. Komm, S. Pearl, G. Marcus, and S. Noach, Opt. Express **27**, 17112 (2019).
11. K. Yang, Y. Yang, J. He, and S. Zhao, *Laser Technology* (IntechOpen, 2019).
12. I. V. Mochalov, Opt. Eng. **36**, 1660 (1997).
13. J. Zhao, Y. Li, S. Zhang, L. Li, and X. Zhang, Opt. Express **23**, 10075 (2015).
14. D. Sebbag, A. Korenfeld, U. Ben-Ami, D. Elooz, E. Shalom, and S. Noach, Opt. Lett. **40**, 1250 (2015).
15. L. E. Batay, A. N. Kuzmin, A. S. Grabtchikov, V. A. Lisinetskii, V. A. Orlovich, A. A. Demidovich, A. N. Titov, V. V. Badikov, S. G. Sheina, V. L. Panyutin, M. Mond, and S. Kück, Appl. Phys. Lett. **81**, 2926 (2002).
16. G. Demetriou, A. J. Kemp, and V. Savitski, Opt. Express **27**, 10296 (2019).
17. V. G. Savitski, Opt. Express **22**, 21767 (2014).
18. D. J. Spence, Prog. Quantum Electron. **51**, 1 (2017).
19. A. Sabella, J. A. Piper, and R. P. Mildren, Opt. Lett. **39**, 4037 (2014).
20. A. Penzkofer, A. Laubereau, and W. Kaiser, Prog. Quantum Electron. **6**, 55 (1979).